Use of the Poisson−Boltzmann Equation To Estimate The Electrostatic Free Energy Barrier for Dielectric Models of Biological Ion Channels

Philip Weetman, Saul Goldman,* and C. G. Gray

Departments of Physics and Chemistry and Biochemistry, University of Guelph, Guelph, Ontario, Canada N1G 2W1

Received: April 3, 1997; In Final Form: May 27, 1997[⊗]

We have obtained the electrostatic free energy profile of a univalent positive ion as it is moved from a bulk electrolyte solution into a biological ion channel of various model forms. The form of the results was unaffected by the method of calculation. We used a fully consistent nonlinearized Poisson−Boltzmann scheme, a fully consistent linearized Poisson−Boltzmann scheme, and a hybrid scheme. The channel models we used were designed to (crudely) mimic the shape and imbedded charge and dipolar distributions for biological ion-selective channels (such as the voltage-gated K^+ "shaker" channel). The results obtained were accounted for on simple physical grounds.

1. Introduction

In a series of papers, Jordan and co-workers[1] have shown how to estimate the electrostatic contribution to the free energy change that accompanies the movement of an ion through a transmembrane ionic channel. It is noteworthy and interesting that the quasi-macroscopic electrostatic models used qualitatively captured the separate contributions to the free energy due to microscopic phenomena such as the removal of an ion from the center of its ion atmosphere (which is excluded from the channel) and by the changing dielectric environment experienced by the ion as it moves from the bulk solution into the channel. Also of interest are the expressions derived by Sharp and Honig[2] for electrostatic free energy changes (in related applications) that are consistent (in a sense to be explained below) with either the linear or nonlinear forms of the Poisson−Boltzmann (PB) equation.

In this article we continue and extend the work of these authors by doing two main things. First, we numerically determine the electrostatic translocation free energy profile of an ion by three routes: the fully nonlinear PB, the fully linear PB, and hybrid method. We did this to determine how sensitive the results were to the method of calculation for ion channel problems. Second, we determined the electrostatic translocation free energies profiles for various dielectric models of an ion channel. We did this to learn about how the answers were influenced by the channel shape and by the presence of fixed charge and fixed dipolar distributions at various locations within the channel. We chose symmetrical and asymmetrical hourglass shapes, and cylindrically symmetric charge and dipolar distributions, in an attempt to roughly mimic various real transmembrane ion-selective channels (such as the "Shaker" voltage-gated K^+ channel[3]).

2. Theory

The Poisson−Boltzmann equation is derived by combining the exact Poisson equation,[4] written in thermally averaged form[5]

$$\nabla\cdot\epsilon(\underline{\mathbf{r}})\langle\nabla\phi(\underline{\mathbf{r}})\rangle + \rho_f(\underline{\mathbf{r}}) + \langle\rho_m(\underline{\mathbf{r}})\rangle = 0 \qquad (1)$$

with the approximate Boltzmann distribution function. To simplify notation, we have divided (1) by 4π so that it does not occur explicitly. Thus, in the equations below $\epsilon(\underline{\mathbf{r}})$ *in vacuo* is taken to be $1/4\pi$ rather than 1. In the applications, when we state $\epsilon_{bulk} = 80$, for example, we have implicitly restored the factor 4π. The Boltzmann distribution function is used to estimate the concentration at location $\underline{\mathbf{r}}$ (relative to a fixed ion (f)) of the mobile ions (m) in the system:

$$\langle\rho_m(\underline{\mathbf{r}})\rangle \equiv \sum_s c_s q_s g_s(\underline{\mathbf{r}})$$

$$g_s(\underline{\mathbf{r}}) \equiv e^{-\beta w_s(\underline{\mathbf{r}})} \approx e^{-\beta q_s\langle\phi(\underline{\mathbf{r}})\rangle} \qquad (2)$$

In (1) and (2), $\epsilon(\underline{\mathbf{r}})$ is the dielectric constant at $\underline{\mathbf{r}}$, which is presumed to be known, $\phi(\underline{\mathbf{r}})$, $\rho_f(\underline{\mathbf{r}})$, and $\rho_m(\underline{\mathbf{r}})$ are respectively the potential, density of fixed charges, and density of mobile charges at $\underline{\mathbf{r}}$, the subscript "s" denotes species type, c, q, g, and w are respectively the bulk concentration, charge, pair correlation function, and potential of mean force, $\beta = 1/kT$ where k is the Boltzmann constant and T is the absolute temperature, and $\langle\ \rangle$ denotes a thermal average. The fixed charges in the present application are of two types: (i) the "central" ion that is systematically moved along the symmetry axis through a series of fixed locations from the outer solution into the channel, through the channel, and out of the other end of the channel and (ii) monopole or dipolar charge distributions that are imbedded at various locations on the channel wall.

Substituting (2) into (1) gives the (full) nonlinearized Poisson−Boltzmann (NLPB) equation

$$\nabla\cdot[\epsilon(\underline{\mathbf{r}})\langle\nabla\phi(\underline{\mathbf{r}})\rangle] = -\rho_f(\underline{\mathbf{r}}) - \sum_s c_s q_s e^{-\beta q_s\langle\phi(\underline{\mathbf{r}})\rangle} \qquad (3)$$

which, for an electrically neutral 1:1 electrolyte solution, simplifies to

$$\nabla\cdot[\epsilon(\underline{\mathbf{r}})\nabla\phi(\underline{\mathbf{r}})] = -\rho_f(\underline{\mathbf{r}}) - ce(e^{-\beta e\phi(\underline{\mathbf{r}})} - e^{\beta e\phi(\underline{\mathbf{r}})}) \qquad (4)$$

$$= -\rho_f(\underline{\mathbf{r}}) + 2ce\sinh(\beta e\phi(\underline{\mathbf{r}}))$$

In (4), c is the bulk concentration (particles/volume) for either species, e is the proton charge, and we have dropped the $\langle\ \rangle$ for simplicity of notation—i.e., $\phi(\underline{\mathbf{r}}) \equiv \langle\phi(\underline{\mathbf{r}})\rangle$ in (4) and hereafter.

* To whom correspondence should be addressed at the Department of Chemistry and Biochemistry.

[⊗] Abstract published in *Advance ACS Abstracts,* July 15, 1997.

S1089-5647(97)01162-0 CCC: $14.00

When $\beta e\phi(\underline{\mathbf{r}})$ is small, the exponent in (4) can be linearized to give the linearized Poisson−Boltzmann (LPB) equation

$$\nabla\cdot[\epsilon(\underline{\mathbf{r}})\nabla\phi(\underline{\mathbf{r}})] = -\rho_f(\underline{\mathbf{r}}) + 2c\beta e^2\phi(\underline{\mathbf{r}}) \tag{5}$$

For semirealistic channel shapes and imbedded charge distributions, (4) or (5) can only be solved numerically for $\phi(\underline{\mathbf{r}})$. Since these numerical solutions are rather demanding in terms of computer time and memory requirements, we sought a computational route from $\phi(\underline{\mathbf{r}})$ to ΔA_{el} (the total electrostatic contribution to the Helmholtz free energy of the system for a particular fixed charge distribution) that was as simple as possible. To this end we chose the route derived by Sharp and Honig[2] who expressed ΔA_{el} as a free energy density integral and used the fact that both the NLPB and the LPB equations can be put into the form of an Euler−Lagrange equation for a variational problem. For the NLPB equation, this leads the following free energy functional:[2]

$$\Delta A_{el} = \int\left[\rho_f(\underline{\mathbf{r}})\,\phi(\underline{\mathbf{r}}) - \frac{2c}{\beta}(\cosh(\beta e\phi(\underline{\mathbf{r}}) - 1) - \epsilon(\underline{\mathbf{r}})\frac{(\nabla\phi(\underline{\mathbf{r}}))^2}{2}\right] d\underline{\mathbf{r}} \tag{6}$$

The key point here is that (6) involves an integration over the volume of the system only. Had we used either a Debye or a Guntleberg approach for the calculation of ΔA_{el} (by which ΔA_{el} is evaluated by a charging integral in which the charges are built up from zero to their full values either simultaneously (Debye) or successively (Guntleberg)), the calculation would have involved integrating over *both* the volume and the charging parameter. By using the free energy functional route, we avoid having to integrate over a charging parameter.

When $\beta e\phi(\underline{\mathbf{r}})$ is small, the cosh() simplifies, giving

$$\Delta A_{el} = \int\left[\rho_f(\underline{\mathbf{r}})\,\phi(\underline{\mathbf{r}}) - c\beta e^2\phi^2(\underline{\mathbf{r}}) - \epsilon(\underline{\mathbf{r}})\frac{(\nabla\phi(\underline{\mathbf{r}}))^2}{2}\right] d\underline{\mathbf{r}} \tag{7}$$

which, by using Gauss' law, further simplifies to

$$\Delta A_{el} = \int\frac{\rho_f(\underline{\mathbf{r}})\,\phi(\underline{\mathbf{r}})}{2}\,d\underline{\mathbf{r}}$$

$$\approx \frac{1}{2}\sum_i q_i(\underline{\mathbf{r}})\,\phi_i(\underline{\mathbf{r}}) \tag{8}$$

where the sum is over all the finite-sized volume elements in the system. Equation 8 is the free energy expression consistent with the LPB equation.

We have used (6) and (8) to provide values for ΔA_{el} consistent with the NLPB and LPB equations, respectively.

It is also possible to evaluate ΔA_{el} by what we call a hybrid expression. This consists of substituting $\phi(\underline{\mathbf{r}})$ obtained from the solution of the NLPB equation (i.e. (4)) into (8). This route was used by Jordan *et al.*[1] and we did some of our calculations in this way in order to check our results.

The inexactness of the PB equation means of course that in the absence of a simulation there is no way of knowing which route provided the best approximation. We shall see, however, that all three routes produced results that were identical in form and were often each within each others' numerical uncertainties.

3. Calculations

Our method of calculation is similar to that of Jordan *et al.*,[1] and therefore the description given here is brief.

The potential is determined by first recasting the Poisson−Boltzmann equation ((4) for the NLPB; (5) for the LPB) into integrated form. The entire system is subdivided into a finite number of cylindrical volume elements, and the equations are recast as volume integrals over these cylindrical volume elements. Volume integrations over the charge density are done analytically, under the assumption that the charge density is uniform over the volume element. Volume integrations over $\nabla\cdot[\epsilon(\underline{\mathbf{r}})\nabla\phi(\underline{\mathbf{r}})]$ are transformed to surface integrals using Gauss' law, and a finite difference approximation is used to approximate the gradient of the potential. In evaluating the surface integrals, use is made of the continuity of the normal component of the dielectric displacement vector across a dielectric boundary, and we assume that the gradient of the potential is constant over the region of integration. Additional details are given in refs 1 and 6. The resultant equations (one for each cylindrical volume element) are solved iteratively for $\phi(\underline{\mathbf{r}})$ under the constraint (boundary condition) that $\phi(\underline{\mathbf{r}})$ vanishes at the edge of our sample.

These equations that relate $\phi(\underline{\mathbf{r}})$ in each cylindrical annulus to those of its nearest neighbors are coupled linearly in the case of the LPB and nonlinearly for the NLPB. The method of solution we used involved an extension of Newton's method of root finding called "relaxation",[7] augmented by an efficiency-enhancing technique called the "multigrid" method.[8] The latter is a device for ensuring reasonable initial guesses of $\phi(\underline{\mathbf{r}})$ on the dielectric grid that is superimposed on the system. Additional details and the full algorithm are given in ref 6.

Once $\phi(\underline{\mathbf{r}})$ has been determined as described above, the calculation of ΔA_{el} is particularly rapid and simple. The same volume elements used for the determination of $\phi(\underline{\mathbf{r}})$ are used again for the calculation of ΔA_{el}. For ΔA_{el} consistent with the NLPB equation, the volume integral in (6) is rewritten as a sum over all the volume elements in the system, with the gradient of the potential replaced by its finite difference approximation. For the LPB we simply use (8).

Rather than use a convergence criterion based on $[\phi^{(i+1)}(\underline{\mathbf{r}}) - \phi^{(i)}(\underline{\mathbf{r}})]$ where the index "i" is the iteration number, we used instead a criterion based on $[\Delta A_{el}^{(i+1)} - \Delta A_{el}^{(i)}]$. We did this because our focus on this work was ΔA_{el} as opposed to $\phi(\underline{\mathbf{r}})$. Thus the iterations were continued until $[\Delta A_{el}^{(i+1)} - \Delta A_{el}^{(i)}] < \delta$ where δ is a preset small number. Typically the iterations—of the order of 1000—were continued until $[\Delta A_{el}^{(i+1)} - \Delta A_{el}^{(i)}]$ was less than $.001\Delta A_{el}^{(i)}$.

The system size was determined by the need for $\phi(\underline{\mathbf{r}})$ to vanish asymptotically (i.e. at large distances). Thus, trial calculations were done for a series increasing system sizes, until the ΔA_{el} values changed by less than 0.1% upon further increases. The sizes of our systems were (radius × length) 80 Å × 80 Å for the 25 Å long channels and 160 Å × 160 Å for the 55 Å long channels described below. We used a grid size of 0.625 Å × 0.625 Å, for which changes in $[\Delta A_{el}^{(i+1)} - \Delta A_{el}^{(i)}]$ dropped to less than 0.1% (for 25 Å long channels) in runs of approximately 30 min on an SGI R4000 level workstation.

We estimate that our reported ΔA_{el} values are never more than 10% from their corresponding asymptotic values, i.e., from the values that would be obtained in the limit of an infinitely fine grid superimposed on an infinitely large sample, with an infinite member of iterations carried out. The largest source of discrepancy between our results and their asymptotic limit stems from our not being able to afford to use grid sizes smaller than 0.625 Å × 0.625 Å. However the accuracy obtained (∼10%) is sufficient for our purposes, which was to generate all the qualitative trends that arise when the channel geometry and embedded charge distributions are altered.

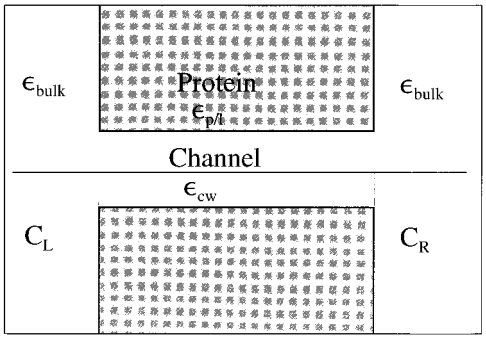

Figure 1. Side view of a right-cylindrical model of an ion channel used to check our results and to assess their sensitivity to the method of calculation. C_L, C_R mean bulk electrolyte concentration on the left and right respectively; only the "central" ion but not bulk electrolyte can enter the channel; the dotted line denotes the boundary between the bulk solution and the channel; $\epsilon_{p/l}$ is the dielectric constant of the protein and lipid considered for our purposes as a homogeneous single substance. The solid horizontal line is the symmetry axis of the system along which the fixed "central" ion is placed. ϵ_{bulk} was taken to be 80 in all our calculations. For this model (that is used to check our calculations) $\epsilon_{p/l} = 2$ and $\epsilon_{CW} = 80$.

TABLE 1: Effect of Method of Calculation on ΔA_{el} for a Cylindrical Channel for Different Central Ion Locations and Bulk Electrolyte Concentrations

electrolyte concn (mol/L) ($C_L = C_R = C$)[a]	z[b] (Å)	$\Delta A_{el}/kT$[c] method of calculation			
		NLPB	LPB	hybrid	ref 1
2.5	0	11.02	9.33	9.33	9.40
2.5	±10	3.76	3.61	3.39	3.47
0.5	0	10.94	9.30	9.27	9.32
0.5	±10	4.39	3.90	3.53	3.63
0.05	0	10.88	9.23	9.22	
0.05	±10	4.72	4.05	3.80	

[a] Equal bulk electrolyte concentrations were used for this test—see Figure 1 for additional details. [b] z is the location on the symmetry axis relative to the center of the channel to which the ion is brought from the bulk of the solution. [c] ΔA_{el} is the electrostatic Helmholtz free energy change that accompanies the translocation of the ion from $\pm\infty$ along the symmetry axis to the location in question; $T = 298.15$ K. See text for the meaning of NLPB, LPB, and hybrid. In keeping with cylindrical symmetry the ion was modeled as a cylinder with radius 1.25 Å, length 2.5 Å, and a valency of +1, i.e., a charge of $+1.6021 \times 10^{-19}$ C. This unit positive charge was uniformly distributed over the cylinder.

4. Results and Discussion

To check our equations, codes, and the adequacy of convergence and to see how the method of calculation influenced the results, we first did a series of calculations for the same model channel, using the same conditions as in ref 1. This was a right-cylindrical channel, 25 Å long and 5 Å in diameter, a side view of which is shown in Figure 1. It has been used in the past as a model for gramicidin. The results of this test calculation are given in Table 1, from which it is seen that our agreement with the results obtained by Jordan *et al.*[1] is excellent. These workers used the hybrid method to obtain ΔA_{el}, and our results from this method agree with theirs to within 3%. Since, as noted above, we estimate that our results can in some instances be as much as 10% away from their asymptotic values, we clearly are in quantitative agreement with work of Jordan *et al.*

Our main interest was to determine whether the approximate approach taken here could qualitatively capture the physical effects expected to arise when the channel shape and its imbedded charge or dipolar distributions were modified to resemble somewhat more closely that of an ion-selective biological ionic channel such as the Shaker voltage-gated K^+ channel. These channels are believed to be shaped somewhat like an hourglass,[3] with the narrowest part of the hourglass acting as the selectivity filter that strongly favors one type of ion over all others for passage. The narrowness of these channels implies that the ions passing through do so in a partially dehydrated state. To compensate the ions for their hydration free energy loss, the channel walls, which are lined with a protein, provide charged or dipolar groups such as carbonyl, carboxylates, or hydroxyls, with which the partially dehydrated ions favorably interact. Therefore we carried out a series of calculations in which the channel was shaped as either a symmetrical or asymmetrical hourglass, and with the channel walls imbedded with fixed dipolar and fixed charge distributions. These distributions were made cylindrically symmetric so as to preserve cylindrical symmetry in our calculations of $\phi(\mathbf{r})$. An hourglass is cylindrically symmetric, so this shape poses no additional computational complexity.

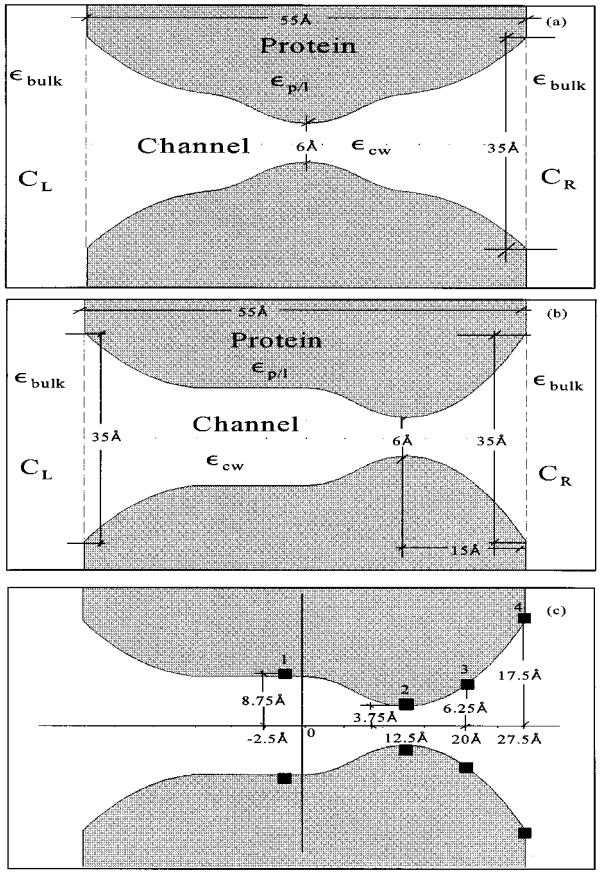

Figure 2. Side views of (a) symmetrical hourglass channel (b) asymmetrical hourglass channel (c) locations at which charged or dipolar annuli are imbedded in the walls of the asymmetrical hourglass model.

A side view of the symmetric and asymmetric hourglass models are shown in Figure 2a,b, and the positions selected for imbedding charged or dipolar annuli in the channel wall are shown in Figure 2c. The equations used to generate these hourglass shapes are for the symmetric case

$$\rho(z) = \begin{cases} 8 + 0.0422(z-15)^2 & 0 < z < 15 \text{ Å} \\ 8 - 0.0644(z-15)^2 & 15 \text{ Å} < z < 21.25 \text{ Å} \\ 3 + 0.0644(z-27.5)^2 & 21.25 \text{ Å} < z < 33.75 \text{ Å} \\ 8 - 0.0644(z-40)^2 & 33.75 \text{ Å} < z < 40 \text{ Å} \\ 8 + 0.0422(z-40)^2 & 40 \text{ Å} < z < 55 \text{ Å} \end{cases} \quad (9)$$

and for the asymmetric case

$$\rho(z) = \begin{cases} 8 + 0.0422(z - 15)^2 & 0 < z < 15 \text{ Å} \\ 8 & 15 \text{ Å} < z < 27.5 \text{ Å} \\ 8 - 0.0644(z - 27.5)^2 & 27.5 \text{ Å} < z < 37.75 \text{ Å} \\ 3 + 0.0644(z - 40)^2 & 33.75 \text{ Å} < z < 55 \text{ Å} \end{cases} \quad (10)$$

In (9) and (10) z is the coordinate along the symmetry axis from the origin, which, for these equations, is centered at the left-most extremity of the channel (shown by a dotted line at the left in Figure 2a,b), and $\rho(z)$ is the distance of the channel wall from the symmetry axis.

For the models used here there are two distinct physical effects that contribute to the free energy change that accompanies the translation of an ion from the bulk solution to the interior of the channel. These are the change in the ion−ion atmosphere interaction energy, which occurs when the ion is partially stripped of its ionic atmosphere when placed in the channel, and the change in the self-energy (or Born solvation energy) of the ion due to the change in its dielectric environment.

The self-energy or Born energy arises from the reversible electrical work required to charge an ion in a continuous medium of dielectric constant ϵ. When an ion is moved from the bulk aqueous solution into a region of different dielectric constant (e.g. in or near the channel), the Born energy changes according to

$$\Delta A_{\text{Born}} \propto \frac{1}{a}\left(\frac{1}{\epsilon_{\text{eff}}} - \frac{1}{\epsilon_{\text{bulk}}}\right) \quad (11)$$

where a is the radius of the ion, ϵ_{bulk} is the dielectric constant of water (here taken as 80), and ϵ_{eff} is the effective dielectric constant experienced by the ion when it is at any location other than the bulk solution. Equation 11 can be regarded as the definition of ϵ_{eff}. While we did not explicitly extract values of ϵ_{eff} from our results, its values are implicit in the values of ΔA_{el}.

As with the work in ref 1, we found the ionic atmosphere effect to be very much smaller than the Born effect. Also, we found the influence of the ionic strength on ΔA_{el} to be similar for cylindrical and hourglass-shaped channels. Consequently our concentration-dependence results offer nothing particularly new, and we focus instead on the results that illustrate the role of channel shape and imbedded charge or dipolar distributions, all done at the same ionic strength (below).

Our results are presented graphically in Figures 3−6. These calculations were all done using (4) and (6), i.e. the NLPB result for $\phi(\mathbf{r})$ used in the expression for ΔA_{el} consistent with the NLPB equation. In all cases $C_{\text{L}} = C_{\text{R}} = 0.50$ mol/L and $\epsilon_{\text{bulk}} = 80$.

The results given in Figure 3 demonstrate the effects on ΔA_{el} due to shape changes on going from a cylinder to a symmetric hourglass to an asymmetric hourglass, and due to changes in the value of the channel water dielectric constant. By the "channel water dielectric constant" we mean the dielectric constant of the water in the channel (for which it is assumed that a macroscopic dielectric constant is applicable). The results are easily understood on physical grounds.

The self-energy of an ion is higher inside the channel than outside, since ϵ_{eff} is lower inside the channel. This is due to the lower dielectric constant of the protein/lipid phase that surrounds the channel and to the lower dielectric constant of the channel water relative to bulk water.[1] For this reason, one would expect the self-energy to peak at the center of a cylindrical channel. It should also peak at the narrowest part of the channel

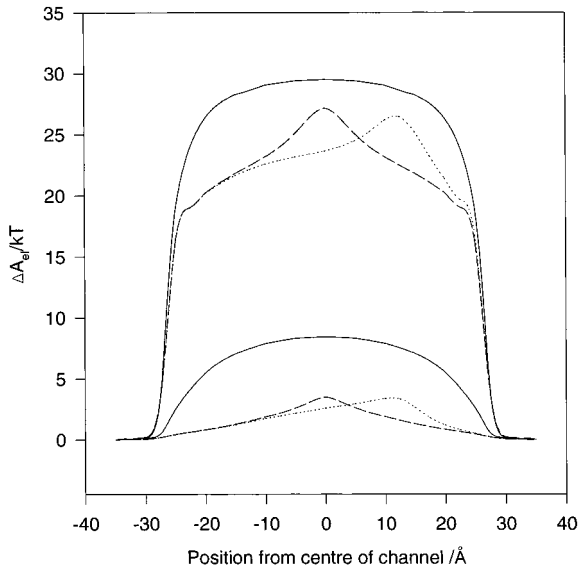

Figure 3. Free energy profiles for 55 Å cylindrical, symmetric, and asymmetric hourglass channels. For all the graphs, $\epsilon_{\text{p/l}} = 4$ and $C_{\text{L}} = C_{\text{R}} = 0.50$ mol/L. The upper graphs are for $\epsilon_{\text{CW}} = 10$; the lower graphs for $\epsilon_{\text{CW}} = 80$. Legend: (—) cylindrical channel, 5 Å diameter; (---) symmetric hourglass channel; (···) asymmetric hourglass channel.

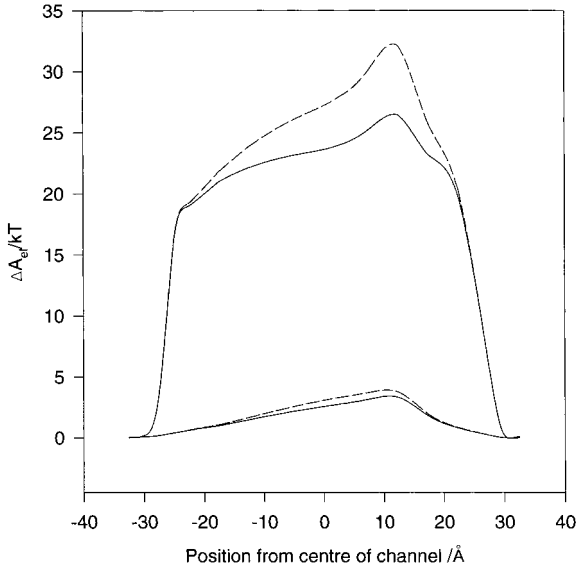

Figure 4. Free energy profiles for 55 Å long asymmetric hourglass channel for different choices of the dielectric constant of the channel water and of the protein/lipid moiety. Upper graphs are for $\epsilon_{\text{CW}} = 10$; lower graphs are for $\epsilon_{\text{CW}} = 80$. Legend: (---) $\epsilon_{\text{p/l}} = 2$; (—) $\epsilon_{\text{p/l}} = 4$.

both for the symmetric and asymmetric hourglass models. These effects are clearly demonstrated in Figure 3. The relatively broad peaks for the cylindrical model result from the relative constancy of ϵ_{eff} over much of the length of the channel. On the other hand, the strictures in the hourglass models imply a relatively narrow minimum in ϵ_{eff} where the strictures occur. This figure also shows that the free energy profile is very sensitive to the value of ϵ_{CW} (the dielectric constant of the channel water). The free energies are much higher for $\epsilon_{\text{CW}} = 10$ than for $\epsilon_{\text{CW}} = 80$. This makes intuitive sense since the choice $\epsilon_{\text{CW}} = 10$ will result in a significantly lower value of ϵ_{eff}, than the choice $\epsilon_{\text{CW}} = 80$. In the latter case, only the somewhat distant protein−lipid moiety with its (selected) value of $\epsilon_{\text{eff}} = 4$, contributes to the lowering of ϵ_{eff} from the bulk solution value of 80.

In Figure 4 we illustrate the influence of the value assigned to the dielectric constant of the protein/lipid phase ($\epsilon_{\text{p/l}}$), for

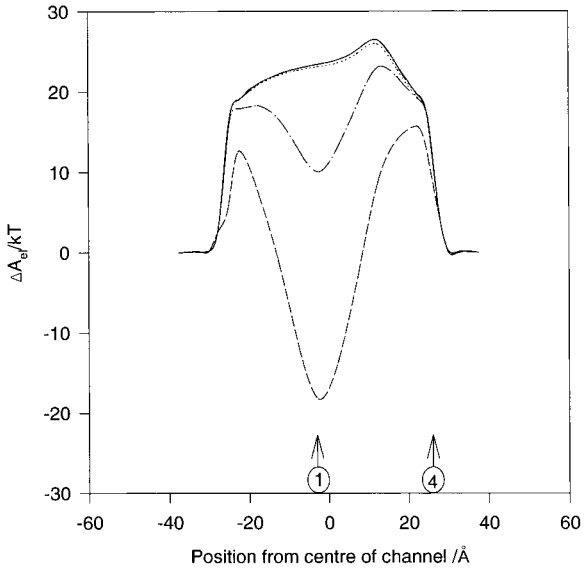

Figure 5. Influence of stabilizing imbedded charged rings and pairs of oppositely charged rings (which we call dipolar rings) placed in the interior and at the mouth of the asymmetric hourglass model. Locations "1" and "4" are shown in Figure 2C. The imbedded distributions are each stabilizing since the central ion is positive, the charged ring (that mimics imbedded charged groups) is negative, and the dipolar rings are placed with the inner ring negative and the outer ring positive. Legend: (—) no imbedded charged or dipolar ring; (---) ring with charge of $-4e$ at position "1"; (—·—) concentric pair of rings (inner with charge $-4e$, outer with charge $+4e$) at position "1"; (···) ring with charge $-4e$ at position "4". The results for a dipolar ring at position "4" were, on the scale used here, not significantly different from the solid line (for no imbedded charged or dipolar rings).

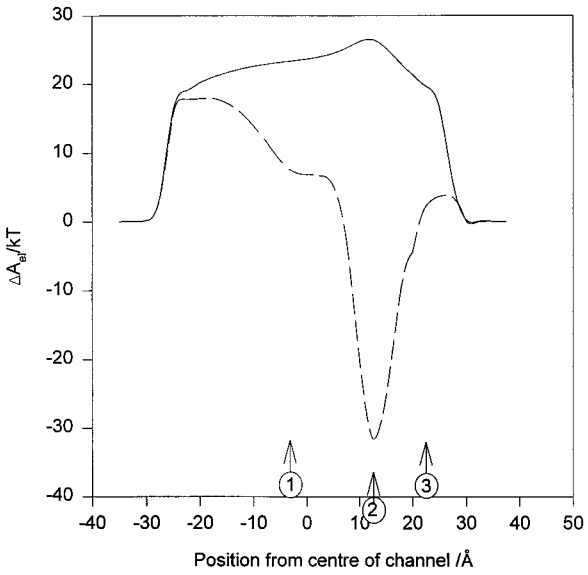

Figure 6. Influence of three stabilizing dipolar rings, simultaneously present, imbedded at locations "1", "2", and "3". Legend: (—) no dipolar rings present; (---) three rings simultaneously present. See legends to Figures 4 and 5 for additional details.

different choices made for the dielectric constant of the channel water (ϵ_{CW}). As expected, the results are quite insensitive to $\epsilon_{p/l}$ for large ϵ_{CW}, but the influence of $\epsilon_{p/l}$ is significant for a low value of ϵ_{CW}. Figure 4 also shows that the value of the maximum in ΔA_{el} can vary by an order-of-magnitude, depending on the choices made for ϵ_{CW} and $\epsilon_{p/l}$.

The results displayed in Figures 5−7 illustrate how charges and dipoles imbedded at selected locations in the channel wall influence the free energy profile of the (positive) central ion. In order to preserve cylindrical symmetry in our calculations,

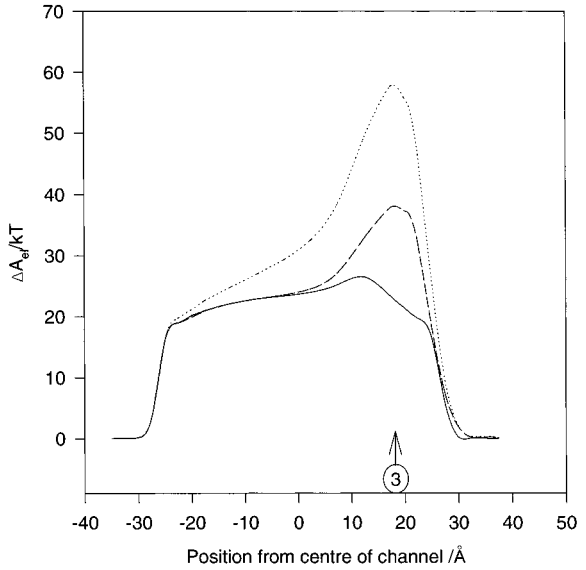

Figure 7. Influence of destabilizing imbedded charged and dipolar distributions. Legend: (—) no imbedded charged or diplar distributions; (---) imbedded destabilizing dipolar distribution at location "3"; (···) imbedded destabilizing charge distribution at location "3". See legends to Figures 4 and 5 for additional details.

we approximated imbedded charges by an imbedded uniformly charged annular ring, and we approximated imbedded dipoles by a pair of concentric, uniformly charged rings (one positive, one negative) imbedded in the channel wall. The calculations are all for the 55 Å asymmetric hourglass model. The locations selected for imbedding these charged rings are shown in Figure 2c; the results are all from the fully consistent NLPB calculations, and in each case $C_L = C_R = 0.50$ mol/L, $\epsilon_{p/l} = 4$, and $\epsilon_{CW} = 10$. The imbedded rings carried a total charge of $\pm 4e$ (where e is the proton charge) uniformly distributed over the volume of the ring, and the ring dimensions were 2.5 Å × 2.5 Å ($\Delta z \times \Delta\rho$); the radius of the inner ring is given for each location in Figure 2c, and the outer ring (for the case of dipoles) had a radius 2.5 Å greater than the inner ring.

The results for imbedded stabilizing charges and dipoles are shown in Figure 5. As expected, the imbedded charged ring in the interior of the channel exerts a very large stabilizing effect, and the imbedded dipolar distribution (with the negative ring closer to the symmetry axis than the positive ring) at this location has a significant but smaller stabilizing effect. Interestingly, the charged ring placed at the mouth of the channel (position 4) exerts only a very small stabilizing influence. This is physically sensible because here ϵ_{eff} is relatively large and the ring is at a considerable distance (≥17.5 Å) from the symmetry axis.

Figure 6 shows the result obtained for three stabilizing dipolar rings, simultaneously present, one at each of positions "1", "2", and "3". Again, the result is easy to understand physically. Each stabilizing dipolar ring produces a drop in ΔA_{el} resulting in a minimum at the z coordinate that corresponds to the center of each ring. By far the largest drop is caused by the dipolar ring imbedded at the narrowest part of the channel-location "2". This ring is expected to have the largest effect both because at location "2", ϵ_{eff} will be smallest and because this dipolar ring is closest to the symmetry axis.

In Figure 7 we show how an imbedded like-charged ring (with charge $+4e$) and an imbedded pair of dipolar rings (with the inner ring positive ($+4e$) and the outer ring negative ($-4e$)) destabilize the free energy profile relative to the channel without imbedded charges or dipoles. Here we get maxima centered at the location of the rings, with the charged ring exerting a greater

influence than the dipolar pair of rings. Again this is exactly what one would expect.

5. Conclusions

(1) We found that the NLPB, LPB, and hybrid methods all give results of the same form when applied to the calculation of the electrostatic free energy change that accompanies the movement of an ion through a variety of models of a biological ion channel. (2) These approximate methods, the imposition of cylindrical symmetry, and the use of "local" dielectric constants remain useful approximations for efficiently providing qualitatively correct trends, even when the models are modified to mimic effects due to channel shape and to imbedded charges or dipoles.

Acknowledgment. We are grateful to the Natural Sciences and Engineering Research Council for financial support and to Dr. Peter Jordan for many helpful discussions and correspondence.

References and Notes

(1) Jordan, P. C.; Bacquet, R. J.; McCammon, J. A.; Tran, P. *Biophys. J.* **1989**, *55*, 1041 and references therein.

(2) Sharp, K. A.; Honig, B. *J. Phys. Chem.* **1990**, *94*, 7684 and references therein.

(3) Hille, B. *Ionic Channels of Excitable Membranes*, 2nd ed.; Sinauer Associates: Sunderland, MA, 1992; p 254.

(4) Arfken, G. *Mathematical Methods for Physicists*, 2nd ed.; Academic Press: New York, 1970; p 65.

(5) McQuarrie, D. A. *Statistical Mechanics*; Harper and Row: New York, 1976; Chapter 15.

(6) Weetman, P. The Use of the Poisson-Boltzmann Equation to Estimate the Free Energy Change Associated with an Ion Going Through Various Models of a Biological Ion Channel. M.Sc. Thesis, University of Guelph, 1997.

(7) Atkinson, K. *Elementary Numerical Analysis*; John Wiley and Sons: New York, 1985.

(8) Press, W. H. Flanery, B. P.; Teukolsky, S. A.; Vetterling, W. T. *Numerical Recipes (Fortran). The Art of Scientific Computing*, 2nd ed.; Cambridge University Press: Cambridge, 1992.